Imaging of Plasmonic Modes of Silver Nanoparticles Using High-Resolution Cathodoluminescence Spectroscopy

Pratik Chaturvedi,[†] Keng H. Hsu,[†] Anil Kumar,[‡] Kin Hung Fung,[†] James C. Mabon,[§] and Nicholas X. Fang[†,*]

[†]Department of Mechanical Science & Engineering, [‡]Department of Electrical and Computer Engineering, and [§]Frederick Seitz Materials Research Laboratory, University of Illinois at Urbana—Champaign, Urbana, Illinois 61801

ARTICLE

ABSTRACT Cathodoluminescence spectroscopy has been performed on silver nanoparticles in a scanning electron microscopy setup. Peaks appearing in the visible range for particles fabricated on silicon substrate are shown to arrive from excitation of out-of-plane eigenmodes by the electron beam. Monochromatic emission maps have been shown to resolve spatial field variation of resonant plasmon mode on length scale smaller than 25 nm. Finite-difference time-domain numerical simulations are performed for both the cases of light excitation and electron excitation. The results of radiative emission under electron excitation show an excellent agreement with experiments. A complete vectorial description of induced field is given, which complements the information obtained from experiments.

KEYWORDS: cathodoluminescence · plasmonics · nanoparticles · extinction · eigenmodes

A multitude of optical phenomena at the nanoscale are made possible by resonant surface plasmons in artificially structured metal systems. These optical phenomena often give rise to properties that are difficult to obtain in natural materials. An entire new generation of artificial materials in the emerging field of plasmonics is designed to harness these properties through nanoscale engineering. These materials find tremendous applications in chemical and biological sensing.[1,2] By simple surface patterning of a thin metal film, it is possible to engineer its surface modes over a wide range of frequencies.[3] Highly localized optical modes associated with patterned surfaces with nanoscale features ($<\sim$200 nm) and the sensitivity of these modes to local refractive index find tremendous potential in realizing compatible and efficient sensors. These optical modes known as localized surface plasmon resonance (LSPR) modes are responsible for producing strong scattering and extinction spectra in metal nanoparticles such as silver and gold. Exploiting local electromagnetic field enhancement associated with these plasmonic structures has led to several interesting applications such as enhanced fluorescence,[4] enhanced photocarrier generation,[5] and other nonlinear effects such as second harmonic[6] and high-harmonic generation.[7] Often the field is confined spatially on length scales on the order of 10−50 nm and varies strongly with particle shape, size, and material composition.[8] Unfortunately, diffraction-limited optical imaging techniques do not have enough spatial resolution to image these plasmon modes or precisely locate the "hot-spots" responsible for producing enormous enhancement. Near-field scanning optical microscopy (NSOM) has been used to investigate these plasmon modes.[9] State-of-the-art NSOM experiments have demonstrated spatial resolution on the order of 15 nm;[10] however, it requires fabrication of very sharp tips. On the other hand, electron beam based characterization techniques such as cathodoluminescence (CL) and electron energy loss spectroscopy (EELS) are able to excite and image plasmon modes with very high spatial resolution. EELS, for example, has been demonstrated to resolve plasmon modes on length scale below 18 nm.[11] EELS technique, however, has to be performed in a transmission electron microscope (TEM), where it detects the inelastically scattered electrons and the loss suffered by electron beam in exciting surface plasmons. Although the technique has been described as one with the best spatial and energy resolution,[11] it requires samples to be electron transparent (typically $<$100 nm). Specialized sample preparation procedure (used for TEM) and instrumentation make it an expensive alternative and infeasible for samples on a thick substrate. On the other hand, scanning electron microscopy (SEM)-based CL technique does not suffer from this limitation. CL (in both SEM and TEM modes) has been utilized to

*Address correspondence to nicfang@illinois.edu.

Received for review May 31, 2009 and accepted September 3, 2009.

Published online September 9, 2009.
10.1021/nn900571z CCC: $40.75

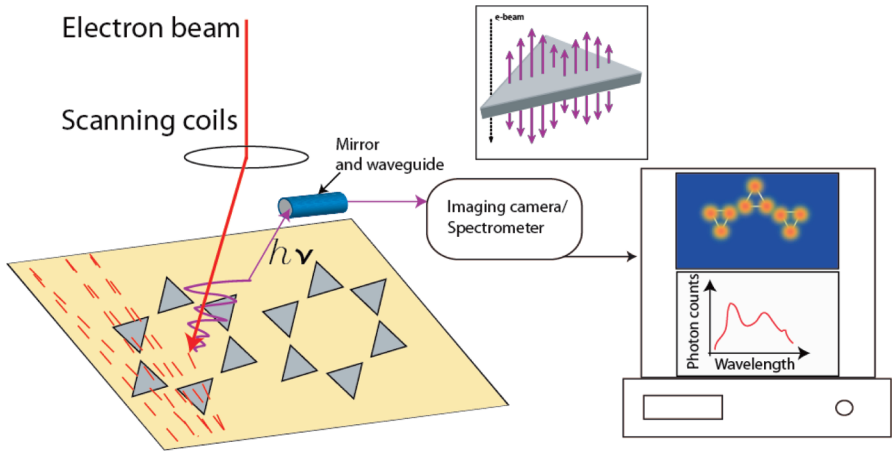

Figure 1. Schematic illustration of CL spectroscopy and imaging technique performed in a scanning electron microscope. Inset: Passing electron beam induces current/electromagnetic oscillations in a metallic particle. These oscillations known as surface plasmon modes are responsible for radiation detected in CL.

image plasmon modes of particles and antennas of various shapes.[12−15]

CL has been used in materials science as an advanced technique for examination of intrinsic structures of semiconductors such as quantum wells[16,17] or quantum dots.[18,19] Typically, a tightly focused beam of electrons impinges on a sample and induces it to emit light from a localized area down to 10−20 nm in size. By scanning the electron beam in an X−Y pattern and measuring the wavelength and intensity of light emitted with the focused electron beam at each point, a high-resolution map of the optical activity of the specimen can be obtained. In traditional cathodoluminescence of semiconductors, impingement of a high-energy electron beam will result in the excitation of valence electrons into the conduction band, leaving behind a hole. The detected photon emission is actually a result of an electron−hole recombination process. In the case of metallic nanostructures, the photons, however, are produced as a result of excited plasmons, that is, collective motion of the conduction electrons induced by the fast moving electrons, and these induced charges can act back on the electron beam, causing it to lose energy as detected in EELS. In CL spectroscopy, we are able to detect radiation due to the oscillating plasmon on metallic structures, allowing quantitative study of the local field (Figure 1). Mechanism of this radiation has recently been presented.[14,20] While photon emission from semiconductor materials on interaction with an electron beam is well-understood, CL from plasmonic nanostructures is a relatively new field and deserves more attention.

In this study, we investigate the plasmon modes of silver (Ag) triangular nanoparticles using CL imaging and spectroscopy. The study is intended to identify the local modes of these nanoparticles. While it is understood that the excitation of plasmons in these metallic nanoparticles is responsible for the field enhancement effect, it is a challenge to identify the local fields associated with these plasmons. Several theoretical studies have identified the plasmon eigenmodes of triangular nanoparticles,[21−23] but only a few experimental studies have demonstrated a resolution capability of mapping the spatial field variation associated with these plasmon modes.[11,24,25] In this work, we report direct excitation and emission of decoupled surface plasmon modes with CL spectroscopy (in SEM chamber) on triangular nanoparticles. In spectroscopic mode with monochromatic photon maps, we are able to distinguish the dramatic spatial variation of resonant plasmon mode on length scales smaller than 25 nm. Numerical simulations were performed to identify the plasmon eigenmodes of triangular particles using a commercial finite-difference time-domain (FDTD) simulator.[26] Both electron beam excitation and a more conventional plane wave scattering type calculations are performed to stress the differences between light excitation and electron excitation. Electron excitation calculations are performed by modeling the moving electron as a series of closely spaced dipoles with temporal phase delay governed by the velocity of the electron. We also incorporate substrate effect into our calculations. Our simulations illustrate that, while normally incident light predominantly excites in-plane eigenmodes, electron beam is more capable of exciting out-of-plane dipole mode of the particles. Under resonance conditions (*i.e.*, at a wavelength of 400 nm), this out-of-plane CL emission mode depicts a standing-plasmon mode pattern.

RESULTS AND DISCUSSION

CL Spectra and Images: Conventionally, nanoparticles are characterized by their extinction spectra. The peaks observed in absorption or scattering spectra of particles under light excitation reveal resonant wavelengths of certain plasmon eigenmodes of the particle. While light excitation can couple to low-frequency plasmon eigenmodes, it is hard to excite high-frequency plasmon states due to large momentum mismatch.[27] Electron excitation on the other hand can couple to high-frequency plasmon modes, and recently, it has been described to directly reveal the local density of plasmon states.[28] While far-field optical techniques are limited in their resolution capability to image the plasmon eigenmodes, electron excitation on the other hand is potentially capable of resolving details below tens of nanometers. Resolving surface plasmon modes and understanding the underlying physics is crucial to de-

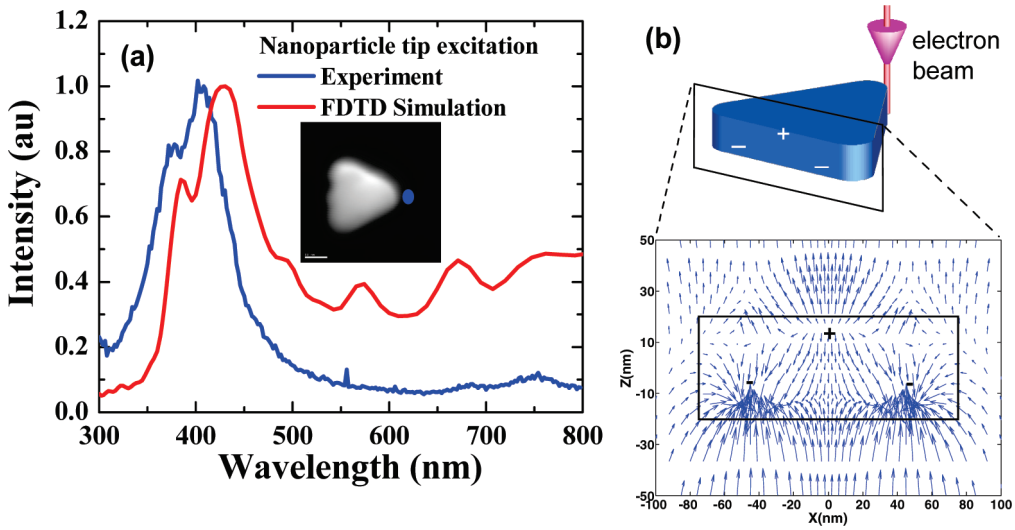

Figure 2. (a) Luminescence spectrum collected from a triangular nanoparticle under tip excitation (blue). The spectrum was corrected for grating response function. Corresponding simulated radiation spectrum (red). Inset: SEM image of the particle with blue dot showing the position of the electron beam. The scale bar is 50 nm. (b) Schematic diagram of the setup for numerical simulation and the corresponding simulated vector plot of the electric field showing an out-of-plane mode excitation at 400 nm wavelength.

sign better plasmonic devices tailored to specific applications.

For the purpose of this study, we fabricated 40 nm thick Ag equilateral triangular nanoparticles with ~200 nm edge length arranged in a hexagonal lattice. These particles are fabricated on a silicon substrate, and the shortest distance between two adjacent particles is >100 nm. Silicon is chosen as the substrate material to suppress background cathodoluminescence in the wavelength range of interest (near-UV and visible). For the purpose of numerical simulations, we model and analyze single nanoparticle. This is because experimentally the interaction distance between electron beam and the particle is limited to a few tens of nanometers, and hence, the excitation of plasmon modes is insensitive to particle coupling over ~100 nm spacing. This is especially true for particles on a nonplasmonic substrate such as silicon. We have performed spectrally resolved CL imaging experiments on these triangular nanoparticles on Si substrate. The emission spectrum of the particle induced by the electron beam passing nearby the tip of the particle reveals a resonance peak at 405 nm and a secondary peak at 376 nm (Figure 2a, blue). This is in excellent agreement with simulations that indicate a resonance peak at 430 nm and secondary peak at 385 nm under tip excitation (Figure 2a, red). A vector plot of the electric field on a vertical plane near the particle shows that the plasmon excited by an electron beam at 400 nm is an out-of-plane mode (Figure 2b). It is to be noted that, in this simulation, the Si substrate has been approximated as nondispersive loss-less material with an average refractive index of 4.8 (see Methods).

Our experimental setup consists of a paraboloidal mirror, which is placed between the sample stage and the electron beam in a SEM chamber. The electron beam passes through an aperture in the mirror to the sample surface. The sample is at the focus of the mirror, which lies 1 mm below it. Light emitted by the sample is collected by the mirror and is directed to the detectors through a light guide. Spectrally resolved measurements are performed using a monochromator (Czerny−Turner-type). Light passing through a monochromator allows taking a spectrum, as well as images, at a selected wavelength. In panchromatic mode of imaging, light skips the monochromator and all of the light is carried to the detection optics. The measurements are performed using a 15 kV electron beam and a photomultiplier tube (PMT) detector with sensitivity encompassing near-ultraviolet (UV) and visible wavelengths (250−850 nm).

Figure 3a is the secondary electron image (SEI) of a triangular nanoparticle, which gives the topographic information about the specimen. Figure 3b is a panchromatic CL image (PanCL). In panchromatic mode, all of the emitted light is collected by the detector and hence the intensity at each pixel represents the integrated photon counts in the sensitivity range of the detector. The PanCL image clearly depicts plasmon-induced luminescence in the Ag nanoparticle. This luminescence arises due to induced electromagnetic field on the nanoparticle caused by the external field of incoming electrons. The way this image is acquired is similar to SEM mapping, that is, by raster scanning the electron beam and collecting emitted photons rather than secondary electrons, as done in scanning electron imaging. The collected light when passed through a grating monochromator allows resolving spectral features, as shown in Figure 2a. As an experimental reference, we have also recorded the emission from flat silver film,

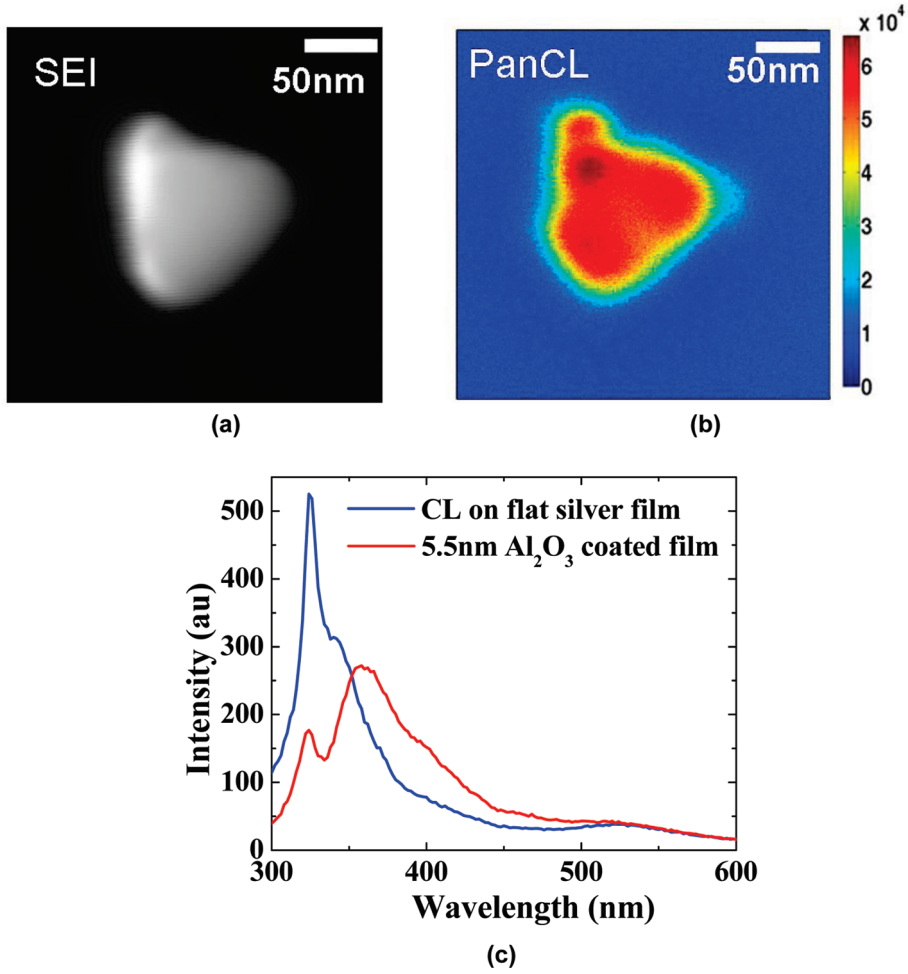

Figure 3. (a) Scanning electron micrograph of the triangular nanoparticle. (b) Panchromatic CL image of the same. (c) Luminescence spectrum collected from a flat silver film.

which reveals a sharp bulk plasmon peak at 325 nm and a surface plasmon peak at 340 nm (Figure 3c, blue). The location of these resonant peaks on flat silver matches with the material permittivity data[29] within ±5 nm. The nature of these peaks (bulk *vs* surface) was further confirmed by a separate CL experiment, where we coated the flat silver film with ~5.5 nm thick alumina (Al_2O_3) coating using atomic layer deposition (ALD). In this case, we observe a sharp peak at 325 nm and a relatively broad peak at 357 nm (Figure 3c, red). This confirms that the peak at 325 nm corresponds to bulk plasmon of silver, whereas the second peak at 340 nm (357 nm) corresponds to surface plasmons at the silver−air (silver−alumina) interface.

Apart from emission spectra, monochromatic photon emission maps are acquired. These monochromatic CL images were obtained by setting the grating monochromator to a specific wavelength and scanning the electron beam over the nanoparticle. These emission maps acquired by raster scanning the electron beam reveal the standing-wave patterns of surface plasmons.[11,12] These standing-wave patterns are observed only under resonance conditions, that is, when the field produced by the electron beam couples strongly to eigenmodes of the particle. Monochromatic CL image obtained at 400 nm wavelength (with a bandwidth of 5.4 nm and 5 ms dwell time at each pixel) shows strong luminescent intensity when the electron beam scans over the tip region of the particle (Figure 4a). An image obtained at a wavelength of 355 nm (Figure 4b) depicts no discernible features in spatial variation of emission, suggesting nonresonant excitation.

Numerical Simulations: While CL experiments are limited to mapping the emitted light intensity by scanning the electron beam, numerical simulations allow us to map the field with fixed electron beam position. It is observed that under resonance conditions the induced electromagnetic field from the electron beam extends across the entire nanoparticle. This is illustrated in Figure 4c, where the electron beam is located near the topmost tip of the particle and the intensity is plotted at 400 nm wavelength. Notice the strong intensity near the tips of the particle, in contrast away from resonance ($\lambda = 355$ nm), the induced field is weak and localized near the probe position (Figure 4d). Hence, the monochromatic emission maps acquired by scanning the electron beam under resonance condition illustrate strong luminescence near the tip regions of the particle and no spatial variation (above the noise level) away from resonance.

It should be noted that the emission pattern obtained at 400 nm wavelength is very similar to the in-plane tip eigenmode of the triangular particle illustrated in earlier theoretical[21,22] and experimental[11,24,25] studies. However, given the dimensions of the particle, the in-plane tip eigenmode occurs at much longer wavelengths. Our simulations indicate that the resonance at 400 nm wavelength corresponds to out-of-plane dipole mode excitation by the electron beam. This is in contrast to light excitation, where a normally incident plane wave predominantly excites an electromagnetic field that corresponds to in-plane charge oscillations. Although, recently, in-plane optical excitation has also been shown to produce out-of-plane modes,[30] an electron beam on the other hand can excite out-of-plane charge oscillations more effectively. This is illustrated in Figure 4e, which plots the simulated vector distribution of the electric field in a plane parallel to the

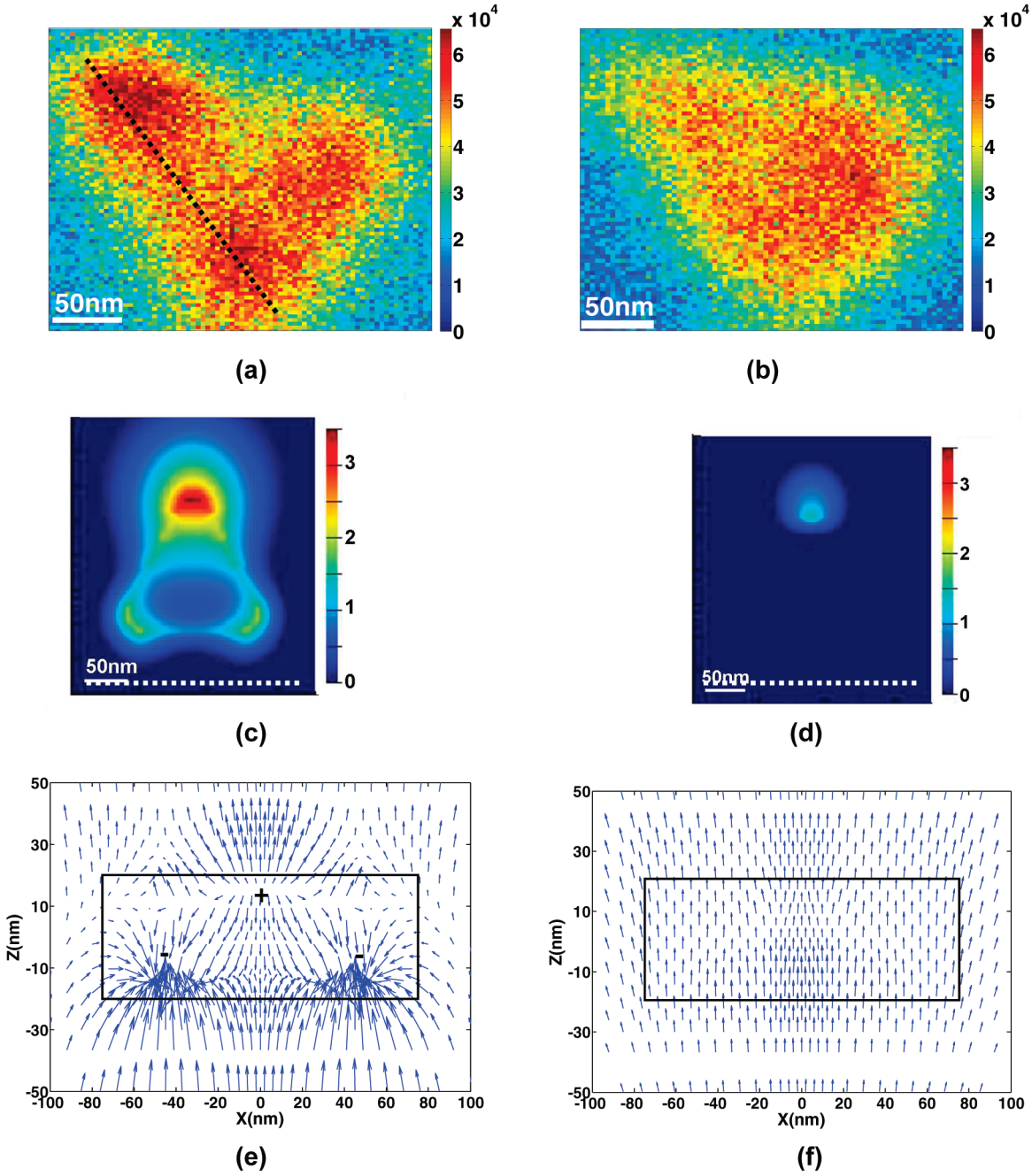

Figure 4. (a) Monochromatic photon emission map acquired at 400 nm wavelength and (b) 355 nm wavelength. (c) Simulated electric field intensity with tip excitation at 400 nm wavelength for the triangular nanoparticle on substrate (n = 4.8). (d) Intensity at 355 nm wavelength. The color scale is in arbitrary units in log scale for (c) and (d). (e) Simulated vector plot of electric field at 400 nm wavelength showing out-of-plane dipole mode excitation. The location of the plane is indicated by the white dotted line in (c). Electron beam travels in the z direction, and the particle boundary is shown by black lines. (f) Vector plot at off-resonance wavelength of 355 nm.

direction of the electron beam. Under nonresonance conditions (λ = 355 nm), the induced field does not show charge oscillations (Figure 4f).

Light Excitation: To further illustrate the differences between light excitation and electron excitation, we have calculated the scattering properties of a triangular nanoparticle under plane wave illumination. When light is resonantly coupled to the plasmon modes of a nanoparticle, it leads to strong scattering and absorption of the incident field. Thus, the resonance modes can be identified based on the extinction spectrum of the particle. Figure 5a presents the extinction spectra of isolated equilateral triangular nanoparticles (200 nm edge length, 40 nm thickness) suspended in air. We observe a dipolar plasmon peak at 677 nm and a quadrupole peak at 400 nm (black curve). The polarity of these peaks is identified based on vectorial description of the polarization response of the particle. These resonant peaks represent the well-known in-plane "tip" (dipole) and "edge" (quadrupole) eigenmodes of the trian-

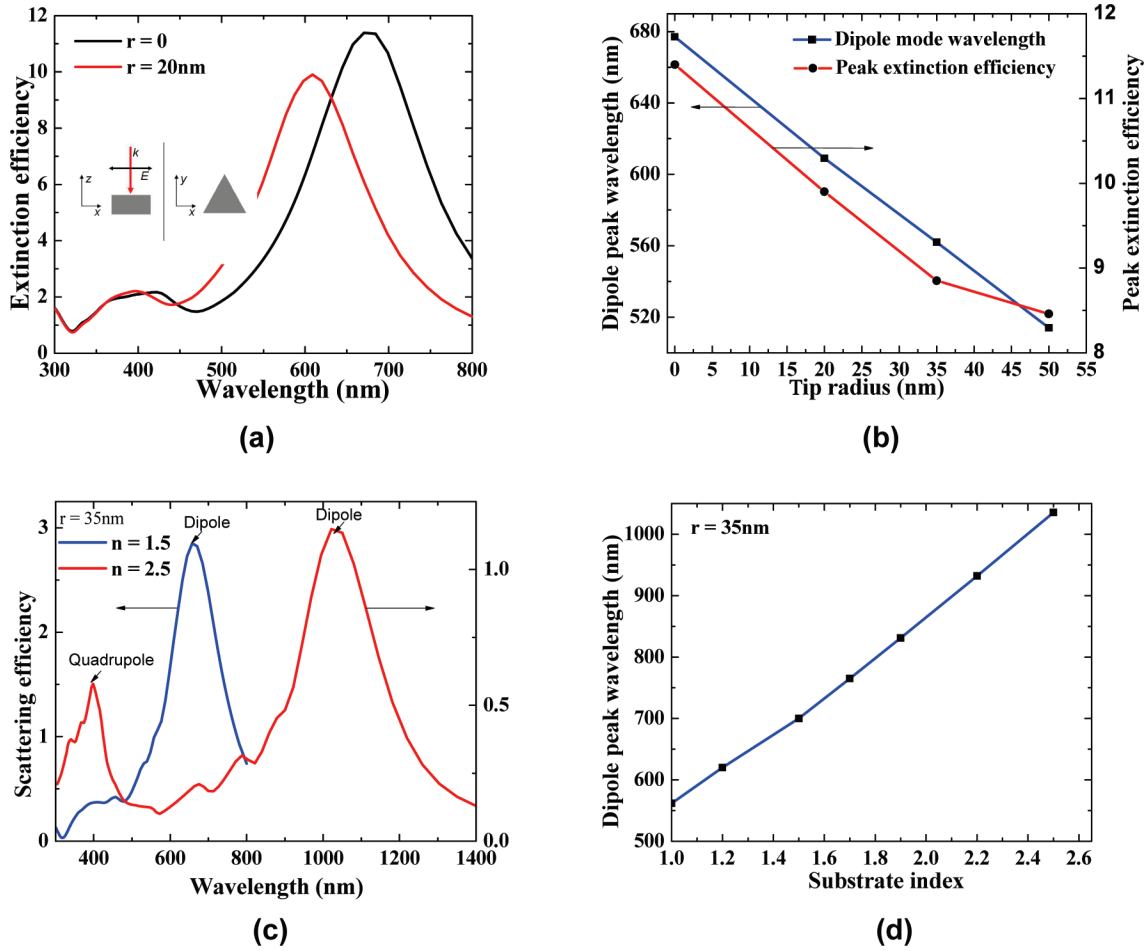

Figure 5. (a) Extinction spectra of triangular nanoparticle and effect of rounding of tips. Inset: Illumination and polarization direction of plane wave. (b) Shift of dipolar resonance and reduction in extinction efficiency with rounding of tips. (c,d) Effect of substrate in plasmon resonances of the particle; *n* refers to the refractive index of the substrate.

gular particle (plane here refers to the plane of the particle).[11,21,31] It is to be noted that this result is for idealistic nanoparticle geometry with sharp tips. Deviation from this geometry such as rounding of tips is known to cause a blue shift of plasmon resonance peaks.[21] This happens because of effective reduction in volume of the particle that leads to reduction in its polarizability. Figure 5a,b illustrates this effect. With a tip radius (*r*) of 20 nm on all corners, a blue shift of 68 nm is observed in dipolar resonance. It is observed that the shift in quadrupole mode is not significant. Rounding of tips also reduces the maximum field enhancement factor, which usually is localized to the corners of the tips. Hence, the peak extinction efficiency also reduces with increasing radius of curvature of tips. It is worth mentioning here that, for a particle with three-fold rotational symmetry, the extinction cross sections under plane wave excitation with two orthogonal polarizations (parallel and perpendicular to the edge of the triangle) are identical at normal incidence. However, the charge oscillations are oriented along the direction of incident polarization.

Next, we consider the effect of substrate. Scattered field characteristics of a particle vary significantly on interaction with a non-homogeneous dielectric environment such as in the presence of a substrate. Figure 5c illustrates this effect where the scattering cross section of triangular particles situated on top of a substrate is plotted. In accordance with experimental setups suitable for light scattering measurements by particles on a substrate, we incorporate light incidence from the top (air side) and only the scattered power in the top half plane is considered in the calculations. Simulated substrate layer extends beyond the perfectly matched layer (PML) boundaries so that it represents a semi-infinite substrate. It is observed that the dipolar resonance of the particle on a substrate red shifts with respect to its free-space resonance (Figure 5d). Qualitatively, the red shift of the resonance can be explained by the increase in the effective permittivity of the surroundings. Particles appear larger with respect to the effective illumination wavelength in high-index surroundings, which causes an increased retardation effect. Thus, for a non-dispersive substrate, the amount of red shift can be roughly approximated by taking the average refractive index of the surroundings. It is worth mentioning that the shift in higher-order resonances, such as quadrupole, is not as significant as the dipolar mode. Hence,

for a high-index substrate, such as silicon, only in-plane quadrupolar resonance is observed (with light excitation) in the visible range for the particle size under consideration.

Electron Excitation: As mentioned before, scattering or extinction spectrum of a particle under plane wave excitation can be significantly different from its CL or EELS spectrum. While a plane wave represents a volumetric excitation source, a highly focused electron beam represents a localized probe which gives information about local density of plasmon states.[28] Furthermore, the two electron characterization techniques also probe different properties of the particle; while EELS measures the total energy loss suffered by the electron in inducing electromagnetic fields on the particle, CL measures only part of the induced field which is radiated out. The two spectra EELS and CL would coincide if there were no losses in the system and the entire induced field is radiated. To numerically investigate the radiative modes that can be excited by a fast moving electron in CL setup, the electron beam can be modeled as a line current density source. The current density due to a moving electron can be written as $\vec{J}(\vec{r},t) = -ev\hat{z}\delta(z - vt)\delta(x - x_0)\delta(y - y_0)$, where e represents electronic charge, v stands for velocity of electron, x_0 and y_0 represent the position of the electron beam, and z is the direction of electron travel. In the FDTD simulation approach, this current density due to a moving charge can be modeled as a series of dipoles with temporal phase delay that is governed by electron velocity (see Methods). The radiative energy component of the induced electromagnetic field is calculated by integrating the Poynting vector normal to an arbitrary large surface in the upper half-plane. Figure 6a presents the radiation spectra of triangular nanoparticle in free-space on excitation with a moving electron charge. Because of the inherent anisotropy of the particle, we model two distinguished cases: (1) when the electron beam is close to the tip of the particle and (2) when it is close to an edge of the particle. It is found that for both of these two cases the main resonance occurring at ~600 nm range (613 nm for tip and 622 nm for edge excitation) corresponds to the in-plane dipolar mode of the nanoparticle, as illustrated in Figure 6b. However, the weaker resonance occurring at ~380 nm corresponds to out-of-plane dipole mode. Since the thickness of the particle is much smaller than its edge length, out-of-plane dipole resonance occurs at a much shorter wavelength compared to in-plane resonance. From the spectra, it is evident that tip excitation is more efficient in exciting in-plane dipolar mode compared to edge excitation. Moreover, when the electron beam is close to the edge of the particle, it also excites in-plane quadrupole mode at 400 nm wavelength, which leads to broadening of the peak observed in the short wavelength range.

We can extend some key observations from plane wave simulations to understand the effect of substrate

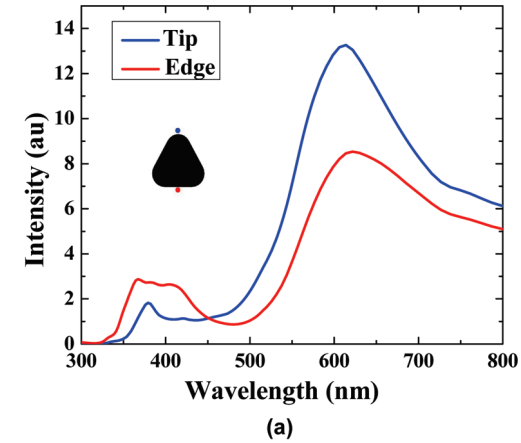

(a)

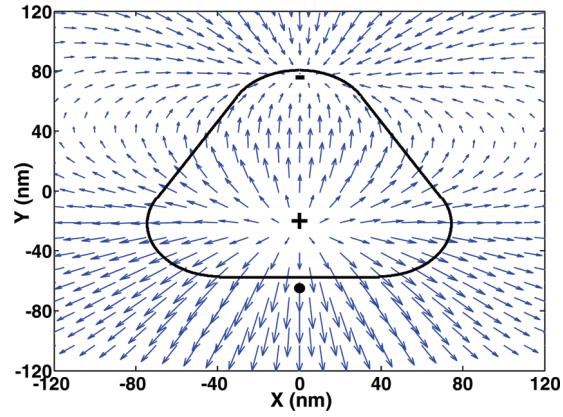

(b)

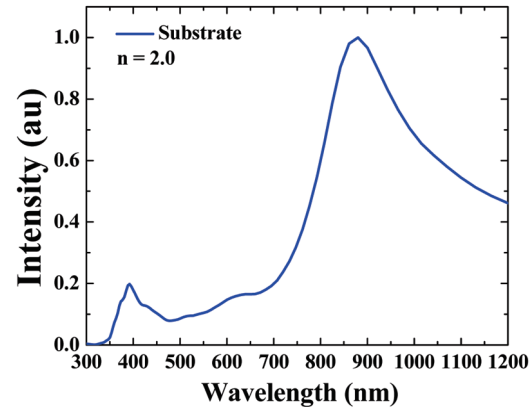

(c)

Figure 6. (a) Simulated radiation spectra of the triangular nanoparticle in free-space upon excitation with electron beam. Inset: Position of the electron beam for tip (blue) and edge (red) excitation cases. (b) Vector plot of electric field for the edge excitation case at 622 nm wavelength, 10 nm away from particle surface showing the excitation of the in-plane dipole mode. The position of the electron beam is marked by a black dot. (c) Effect of substrate on particle resonance upon excitation with electron beam (tip excitation). The substrate is assumed to be of constant refractive index $n = 2$.

on particle resonance under electron excitation. The in-plane dipole mode should red shift because of an increase in the index of the surroundings. This is indeed observed from simulations (Figure 6c). The shift in out-of-plane dipolar mode is not as significant. This is ex-

pected since the thickness of the particle is small, the out-of-plane modes experience lower retardation effects. This suggests that, for these triangular nanoparticles fabricated on high-index substrates such as silicon, electron beam can predominantly excite out-of-plane dipole mode and in-plane quadrupole mode in the visible wavelength range. This is indeed observed in our CL experiments and simulations. The experimentally observed spectrum shows some minor differences compared to simulations (Figure 2a). This may be attributed to the approximations we have made in our simulations. In the electron excitation case, we did not include the dispersive properties of silicon substrate in our simulations. Second, in simulations, the radiation spectra consist of photons integrated over the entire top half space. In our experiments, the collection angle of the mirror is limited to a cone angle of 160°. In light of these differences, the experimental spectrum is in good agreement with simulations.

Resolution: It is evident that the CL technique allows high-resolution mapping of plasmon modes. The quantification of the optical resolution of the technique deserves special attention. It may seem that the resolution of the technique would ultimately be limited only by electron beam diameter, as in the case of secondary electron images, but this may not be the case. In secondary electron imaging, the incoming electron beam knocks off low-energy secondary electrons (<50 eV); the physical nature of this process allows high-resolution topographic image acquisition (1−5 nm). However, in CL imaging, photon emission can occur even when the electron beam is at a distance away from the particle. Electron beam can induce luminescence in a structure without physically passing through it, as indicated by our simulations. As a rough estimate, for 15 keV electron beam, this interaction length can be as large as 18 nm for light emitted at 400 nm wavelength.[14] To estimate resolution, we fit Gaussian functions to the emission eigenmode at 400 nm wavelength. A clear spatial modulation (25% change in normalized intensity) of the eigenmode above the noise level is detectable on a length scale as short as 25 nm. This is illustrated in Figure 7, which plots the variation of radiation intensity along the edge of the particle as marked in Figure 4a.

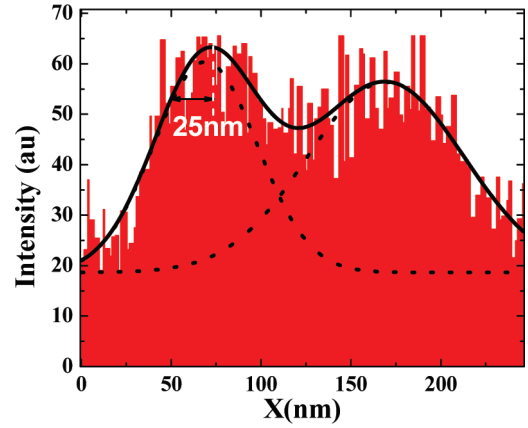

Figure 7. Variation of cathodoluminescence emission along the edge of the particle (marked in Figure 4a) at 400 nm wavelength.

CONCLUSIONS

In this work, CL imaging technique was utilized to image plasmon modes of Ag triangular nanoparticles with high spatial (~25 nm) and spectral resolution (~5.4 nm). Spectroscopic analysis when combined with monochromatic imaging helps us to identify different channels of plasmon-associated photon emission. The process of radiative emission from plasmon in the CL setup was modeled using FDTD approach. Simulations indicate that, in contrast to light excitation, electron beam excites not only the in-plane eigenmodes of nanoparticles but also the out-of-plane modes. Because of the inherent anisotropy of the triangular particle, the position of the electron beam also influences the excitation of eigenmodes. This was presented in the context of "tip" and "edge" excitation of the particle. These results provide a better understanding of excitation and imaging of plasmon modes using CL spectroscopy.

METHODS

Fabrication: For the purpose of this study, Ag nanostructures were fabricated on silicon substrate. The samples were fabricated using a novel solid-state superionic stamping (S4) process.[32,33] This process utilizes a prepatterned stamp made of a superionic conductor such as silver sulfide which supports a mobile cation (silver). The stamp is brought into contact with a substrate coated with a thin silver film. On the application of an electrical bias with the substrate as anode and a metallic electrode at the back of the stamp as cathode, a solid-state electrochemical reaction takes place only at the actual contact at the interface. This reaction progressively removes a metallic layer of the substrate at the contact area with the stamp. Assisted by a nominal pressure to maintain electrical contact, the stamp gradually progresses into the substrate, generating a pattern in the silver film complementary to the prepatterned features on the stamp. Silver sulfide stamps were patterned using focused ion beam technique. A very thin (~2 nm) chromium (Cr) layer is used as the adhesion layer for silver film on silicon. The fabricated structures are coated conformally with very thin dielectric layer (anatase TiO_2, 5 monolayer ~ 2.5 Å) using atomic layer deposition (ALD) to protect the samples from environmental and electron beam damage. Excellent pattern transfer fidelity of the S4 approach down to sub-50 nm resolution and ambient operating conditions make this process suitable for low-cost, high-throughput patterning of plasmonic nanostructures, such as presented in this study.

Simulation: ***Light Excitation:*** To numerically compute absorption and scattering by triangular nanoparticles, we utilize the total-field scattered-field (TFSF) formulation with FDTD approach. In this approach, the computation region is divided into two sections—one where the total field (incident + scattered) is computed and the second where only scattered field is computed. The particles are excited by a normal incident plane wave.

Absorption and scattering cross sections are computed by monitoring the net power inflow in the total-field region near the particle and net power outflow in the scattered field region, respectively. Extinction cross section is the sum of absorption and scattering cross section of the particle. Our numerical calculations suggest that for Ag nanoparticles scattering is approximately an order of magnitude larger than absorption. The material properties used in the calculation are obtained from generalized multicoefficient model[26] that fits the dispersion data obtained from Palik.[34] This approach is more accurate for broadband simulations than fitting a single material model such as Drude or Lorentz.

Electron Excitation: The electron beam has been modeled as a series of closely spaced dipoles each with temporal phase delay according to the velocity of the electron beam. In the absence of any structure, electron beam moving at a constant velocity does not generate any radiation. In FDTD, however, we simulate only a finite portion of the electron path, and the sudden appearance and disappearance of the electron will generate radiation. To solve this problem, we run a second reference simulation where all of the structures are removed, and we can calculate the electromagnetic fields at any wavelength by taking the difference in fields between the simulations.[26] To get an accurate difference, we force the simulation mesh to be exactly the same with and without the structure. Currently, the methodology does not permit the electron beam to pass through a lossy or dispersive substrate material. Further work in this direction is currently underway.

Acknowledgment. The authors are thankful to Dr. Jun Xu of the University of Illinois for several informal discussions. The authors also acknowledge the technical support and assistance received from James Pond and Chris Kopetski of Lumerical Solutions Inc. Cathodoluminescence experiments were carried out in the Frederick Seitz Materials Research Laboratory Central Facilities, University of Illinois, which are partially supported by the U.S. Department of Energy under Grants DE-FG02-07ER46453 and DE-FG02-07ER46471. The authors are grateful for the financial support from the Defense Advanced Research Projects Agency (Grant HR0011-05-3-0002), Office of Naval Research (Grant N00173-07-G013), and National Science Foundation (Grant CMMI-0709023).

REFERENCES AND NOTES

1. Haes, A. J.; Van Duyne, R. P. A Nanoscale Optical Blosensor: Sensitivity and Selectivity of an Approach Based on the Localized Surface Plasmon Resonance Spectroscopy of Triangular Silver Nanoparticles. *J. Am. Chem. Soc.* **2002**, *124*, 10596–10604.
2. McFarland, A. D.; Van Duyne, R. P. Single Silver Nanoparticles as Real-Time Optical Sensors with Zeptomole Sensitivity. *Nano Lett.* **2003**, *3*, 1057–1062.
3. Pendry, J. B.; Martin-Moreno, L.; Garcia-Vidal, F. J. Mimicking Surface Plasmons with Structured Surfaces. *Science* **2004**, *305*, 847–848.
4. Bharadwaj, P.; Novotny, L. Spectral Dependence of Single Molecule Fluorescence Enhancement. *Opt. Express* **2007**, *15*, 14266–14274.
5. Ishi, T.; Fujikata, J.; Makita, K.; Baba, T.; Ohashi, K. Si Nano-Photodiode with a Surface Plasmon Antenna. *Jpn. J. Appl. Phys., Part 2* **2005**, *44*, L364–L366.
6. Eftekhari, F.; Gordon, R. Enhanced Second Harmonic Generation from Noncentrosymmetric Nanohole Arrays in a Gold Film. *IEEE J. Sel. Top. Quantum Electron.* **2008**, *14*, 1552–1558.
7. Kim, S.; Jin, J. H.; Kim, Y. J.; Park, I. Y.; Kim, Y.; Kim, S. W. High-Harmonic Generation by Resonant Plasmon Field Enhancement. *Nature* **2008**, *453*, 757–760.
8. Haes, A. J.; Haynes, C. L.; McFarland, A. D.; Schatz, G. C.; Van Duyne, R. R.; Zou, S. L. Plasmonic Materials for Surface-Enhanced Sensing and Spectroscopy. *MRS Bull.* **2005**, *30*, 368–375.
9. Yin, L.; Vlasko-Vlasov, V. K.; Rydh, A.; Pearson, J.; Welp, U.; Chang, S. H.; Gray, S. K.; Schatz, G. C.; Brown, D. B.; Kimball, C. W. Surface Plasmons at Single Nanoholes in Au Films. *Appl. Phys. Lett.* **2004**, *85*, 467–469.
10. Hartschuh, A.; Qian, H. H.; Meixner, A. J.; Anderson, N.; Novotny, L. Nanoscale Optical Imaging of Excitons in Single-Walled Carbon Nanotubes. *Nano Lett.* **2005**, *5*, 2310–2313.
11. Nelayah, J.; Kociak, M.; Stephan, O.; de Abajo, F. J. G.; Tence, M.; Henrard, L.; Taverna, D.; Pastoriza-Santos, I.; Liz-Marzan, L. M.; Colliex, C. Mapping Surface Plasmons on a Single Metallic Nanoparticle. *Nat. Phys.* **2007**, *3*, 348–353.
12. Gomez-Medina, R.; Yamamoto, N.; Nakano, M.; Abajo, F. J. G. Mapping Plasmons in Nanoantennas *via* Cathodoluminescence. *New J. Phys.* **2008**, *10*, 105009.
13. Hofmann, C. E.; Vesseur, E. J. R.; Sweatlock, L. A.; Lezec, H. J.; Garcia de Abajo, F. J.; Polman, A.; Atwater, H. A. Plasmonic Modes of Annular Nanoresonators Imaged by Spectrally Resolved Cathodoluminescence. *Nano Lett.* **2007**, *7*, 3612–3617.
14. Yamamoto, N.; Araya, K.; de Abajo, F. J. G. Photon Emission from Silver Particles Induced by a High-Energy Electron Beam. *Phys. Rev. B* **2001**, *64*, 205419.
15. Yamamoto, N.; Nakano, M.; Suzuki, T. Light Emission by Surface Plasmons on Nanostructures of Metal Surfaces Induced by High-Energy Electron Beams. *Surf. Interface Anal.* **2006**, *38*, 1725–1730.
16. Cibert, J.; Petroff, P. M.; Dolan, G. J.; Pearton, S. J.; Gossard, A. C.; English, J. H. Optically Detected Carrier Confinement to One and Zero Dimension in Gaas Quantum Well Wires and Boxes. *Appl. Phys. Lett.* **1986**, *49*, 1275–1277.
17. Chichibu, S.; Wada, K.; Nakamura, S. Spatially Resolved Cathodoluminescence Spectra of Ingan Quantum Wells. *Appl. Phys. Lett.* **1997**, *71*, 2346–2348.
18. Leon, R.; Petroff, P. M.; Leonard, D.; Fafard, S. Spatially Resolved Visible Luminescence of Self-Assembled Semiconductor Quantum Dots. *Science* **1995**, *267*, 1966–1968.
19. Rodriguez-Viejo, J.; Jensen, K. F.; Mattoussi, H.; Michel, J.; Dabbousi, B. O.; Bawendi, M. G. Cathodoluminescence and Photoluminescence of Highly Luminescent CdSe/ZnS Quantum Dot Composites. *Appl. Phys. Lett.* **1997**, *70*, 2132–2134.
20. Garcia de Abajo, F. J.; Howie, A. Relativistic Electron Energy Loss and Electron-Induced Photon Emission in Inhomogeneous Dielectrics. *Phys. Rev. Lett.* **1998**, *80*, 5180.
21. Shuford, K. L.; Ratner, M. A.; Schatz, G. C. Multipolar Excitation in Triangular Nanoprisms. *J. Chem. Phys.* **2005**, *123*, 114713.
22. Hao, E.; Schatz, G. C. Electromagnetic Fields around Silver Nanoparticles and Dimers. *J. Chem. Phys.* **2004**, *120*, 357–366.
23. Martin, O. J. F. Plasmon Resonances in Nanowires with a Non-Regular Cross-Section. In *Optical Nanotechnologies*; Tominaga, J., Tsai, D. P., Eds.; Springer-Verlag: Berlin, Heidelberg, 2003; pp 183−210.
24. Nelayah, J.; Gu, L.; Sigle, W.; Koch, C. T.; Pastoriza-Santos, I.; Liz-Marzán, L. M.; van Aken, P. A. Direct Imaging of Surface Plasmon Resonances on Single Triangular Silver Nanoprisms at Optical Wavelength Using Low-Loss EFTEM Imaging. *Opt. Lett.* **2009**, *34*, 1003–1005.
25. Rang, M.; Jones, A. C.; Zhou, F.; Li, Z. Y.; Wiley, B. J.; Xia, Y. N.; Raschke, M. B. Optical Near-Field Mapping of Plasmonic Nanoprisms. *Nano Lett.* **2008**, *8*, 3357–3363.
26. http://www.lumerical.com/.
27. Raether, H. *Surface-Plasmons on Smooth and Rough Surfaces and on Gratings*; Springer: Berlin, 1988; Vol. 111, pp 1−133.
28. Garcia de Abajo, F. J.; Kociak, M. Probing the Photonic Local Density of States with Electron Energy Loss Spectroscopy. *Phys. Rev. Lett.* **2008**, *100*, 106804.
29. Johnson, P. B.; Christy, R. W. Optical Constants of Noble Metals. *Phys. Rev. B* **1972**, *6*, 4370–4379.
30. Hubert, C.; Bachelot, R.; Plain, J.; Kostcheev, S.; Lerondel, G.; Juan, M.; Royer, P.; Zou, S. L.; Schatz, G. C.; Wiederrecht,

G. P.; *et al.* Near-Field Polarization Effects in Molecular-Motion-Induced Photochemical Imaging. *J. Phys. Chem. C* **2008**, *112*, 4111–4116.
31. Sherry, L. J.; Jin, R. C.; Mirkin, C. A.; Schatz, G. C.; Van Duyne, R. P. Localized Surface Plasmon Resonance Spectroscopy of Single Silver Triangular Nanoprisms. *Nano Lett.* **2006**, *6*, 2060–2065.
32. Hsu, K. H.; Schultz, P. L.; Ferreira, P. M.; Fang, N. X. Electrochemical Nanoimprinting with Solid-State Superionic Stamps. *Nano Lett.* **2007**, *7*, 446–451.
33. Chaturvedi, P.; Hsu, K.; Zhang, S.; Fang, N. New Frontiers of Metamaterials: Design and Fabrication. *MRS Bull.* **2008**, *33*, 915–920.
34. Palik, E. D. *Handbook of Optical Constants*; Academic Press: New York, 1984.